

## A regional ocean modeling system for the Long-term Ecosystem Observatory

John L. Wilkin, Hernan G. Arango, Dale B. Haidvogel, C. Sage Lichtenwalner,<sup>1</sup>  
 Scott M. Glenn, and Katherine S. Hedström<sup>2</sup>

Institute of Marine and Coastal Sciences, Rutgers University, New Brunswick, New Jersey, USA

Received 20 November 2003; revised 5 February 2005; accepted 14 March 2005; published 28 June 2005.

[1] A coastal ocean forecasting system was developed for the Long-term Ecosystem Observatory (LEO) on New Jersey's inner shelf. The forecast system comprised an ocean model, the Regional Ocean Modeling System, forced by a high-resolution atmospheric forecast, with assimilation of ocean data from ships and coastal radar systems. The forecasts were used to aid the deployment of real-time adaptive sampling observing systems during the July 2001 Coastal Predictive Skill Experiment. Temperature and salinity assimilation data were prepared by optimal interpolation of shipboard towed-body data. Surface current observations from coastal radar were projected vertically for assimilation using a statistically based extrapolation. The assimilation methods tested with the operational forecast system in July 2001 were continuous nudging and intermittent melding of the model forecast and gridded data. Observations from a validation array of current meter and thermistor moorings deployed on a cross-shore line through the center of the LEO intensive observing area were used to formulate a set of quantitative model skill metrics that focused on aspects of the two-layer wind-driven upwelling and downwelling circulation that characterizes ocean dynamics during the stratified summer season along this coast. An ensemble of model and data assimilation configurations were tested, showing that the  $k$  profile parameterization for vertical turbulence closure, and assimilation by intermittent melding, comprised the forecast system with the more significant skill as measured by the mean squared error of the validation metric time series.

**Citation:** Wilkin, J. L., H. G. Arango, D. B. Haidvogel, C. S. Lichtenwalner, S. M. Glenn, and K. S. Hedström (2005), A regional ocean modeling system for the Long-term Ecosystem Observatory, *J. Geophys. Res.*, *110*, C06S91, doi:10.1029/2003JC002218.

### 1. Introduction

[2] Coastal ocean modeling efforts at the Rutgers University Long-term Ecosystem Observatory (LEO) have focused on the development and validation of a relocatable coastal ocean forecasting capability. During the Coastal Predictive Skill Experiment (CPSE) at LEO during the summer of 2001, a regional ocean forecasting system was implemented consisting of an ocean model forced by a high-resolution atmospheric forecast, with assimilation of ocean data from towed-body temperature and salinity observations and surface currents from a combination of high-resolution and long-range radar systems. Ensembles of atmosphere and ocean forecasts were generated twice per week for four consecutive weeks from 11 July through 7 August 2001. These predictions were incorporated into the decision making process for the scheduling of ship-

based observations during each subsequent 3 day forecast period, so as to adapt the subsurface sampling network to the evolving circulation.

[3] Here we describe the elements of the modeling and data assimilation system as implemented at LEO during July–August 2001. Quantitative validation metrics are formulated and used to evaluate the model performance at simulating the upwelling and downwelling circulations that were the focus of bio-optical and ecosystem observational programs during the CPSE.

### 2. Forecast System Overview

[4] The LEO coastal ocean forecast system was comprised of a three-dimensional ocean circulation model, the Regional Ocean Modeling System (ROMS), forced with predicted atmospheric marine boundary layer conditions from the U.S. Navy's Coupled Ocean Atmosphere Mesoscale Prediction System (COAMPS) model operated in a multiply nested configuration to produce very high resolution forecasts for the New Jersey coast. Simple yet practical data assimilation schemes were used to reinitialize the ocean model prior to each forecast cycle using data available in real time from a distributed observing network

<sup>1</sup>Now at College of Marine Science, University of South Florida, St. Petersburg, Florida, USA.

<sup>2</sup>Now at Arctic Regions Supercomputing Center, Fairbanks, Alaska, USA.

<ul style="list-style-type: none"> <li>- Free surface, hydrostatic primitive equations model in terrain-following coordinates</li> <li>- Horizontal finite differences and vertical finite volume discretization</li> <li>- 3<sup>rd</sup>-order upstream-biased advection [Shchepetkin and McWilliams, 1998]</li> <li>- Pressure gradient and equation of state give reduced <math>\sigma</math>-coordinate truncation error [Shchepetkin and McWilliams, 2003]</li> <li>- 3<sup>rd</sup>-order predictor/corrector time stepping</li> <li>- Split-explicit time-stepping of barotropic and baroclinic modes constrained for conservation of volume and tracer constancy [Shchepetkin and McWilliams 2005]</li> <li>- Radiation open boundary conditions [Marchesiello et al. 2001]; 1-way embedding in exterior domains</li> </ul>	<ul style="list-style-type: none"> <li>- Synchronous Lagrangian particle tracking</li> <li>- Vertical turbulence closures (see Warner et al. [2005]): KPP [Large et al. 1994, Durski et al. 2004] and the Generalized Length Scale scheme of Umlauf and Burchard [2003] encompassing <math>k</math>-<math>\epsilon</math>, <math>k</math>-<math>\omega</math>, <math>k</math>-<math>\tau</math> and Mellor-Yamada [1982]</li> <li>- Intermittent sub-optimal melding assimilation</li> <li>- Tangent linear and adjoint models for variational assimilation (4D-var, representers), ensemble forecasting and sensitivity analyses [Moore et al. 2004]</li> <li>- Atmospheric, oceanic, and benthic wave-current boundary layers [Keen and Glenn 1995]</li> <li>- Coupled ecosystem (11-component NPZD-carbon, and 61-component EcoSim bio-optics) and sediment transport (USGS Community Model) modules</li> </ul>
--	--

**Figure 1.** Regional Ocean Modeling System (ROMS) model features.

of coastal radar and vessels equipped with ship-to-shore radio modems for the telemetry of towed-body subsurface observations.

### 2.1. Regional Ocean Modeling System (ROMS) Ocean Model Configuration

[5] ROMS is a free-surface primitive equation ocean model being used by a broad community for applications from the basin to coastal and estuarine scales [e.g., Haidvogel et al., 2000; Marchesiello et al., 2003; Lutjeharms et al., 2003; Peliz et al., 2003; Dinniman et al., 2003; MacCready and Geyer, 2001]. Shchepetkin and McWilliams [1998, 2003, 2005] describe in detail the algorithms that comprise the ROMS computational kernel. These include careful formulation of the time-stepping algorithm to allow both exact conservation and constancy preservation for tracers, while achieving enhanced stability and accuracy in coastal applications where the free surface displacement is a significant fraction of the total water depth. Conservative parabolic-spline discretization in the vertical reduces the pressure gradient truncation error that has previously plagued terrain-following coordinate models. Present ROMS features are summarized briefly in Figure 1, though not all these features were implemented at the time of the LEO CPSE forecasting.

[6] The model domain covers the New York Bight and New Jersey shelf (Figure 2). The curvilinear boundary-fitted grid has an average resolution of 1 km, with enhanced grid resolution of approximately 300 m in the vicinity of the 30 km by 30 km LEO intensive observing area adjacent to the Rutgers University Marine Field Station (RUMFS) at Tuckerton, New Jersey. The bathymetry is from the National Geophysical Data Center 3-arc-second Coastal Relief Model smoothed with two passes of a Shapiro filter to remove wavelengths on the order of the grid scale. Beyond the shelf break, in the southeast corner of the domain, depths greater than 100 m are truncated to 100 m to reduce the CFL constraint on model time step since the focus of the study was locally wind-forced variability near the coast in the LEO vicinity. Tidal sea level and depth average velocity variability were imposed at the domain perimeter using the seven most significant harmonics ( $M_2$ ,  $N_2$ ,  $S_2$ ,  $K_1$ ,  $O_1$ ,  $M_4$ ,  $M_6$ ) from an ADCIRC model simulation of the western Atlantic [Luettich et al., 1992]. The predominant tide component,  $M_2$ , enters the New Jersey Bight as a plane

wave perpendicular to the shelf break. Consequences of truncating the model bathymetry for computational convenience are that (1) the tidal energy flux is underestimated by approximately a factor of four in the southeast corner of the domain and (2) the reduced wave speed in shallower water introduces a phase error of about 30 min. Observed tidal velocities in the LEO region are of order  $5 \text{ cm s}^{-1}$  [Chant et al., 2004] which is a factor of five less than typical wind-driven currents at LEO. Given the dominance of wind-driven variability over tidal forcing at LEO, we consider inaccuracies in the modeled tides are not a serious limitation for the purposes of the present study.

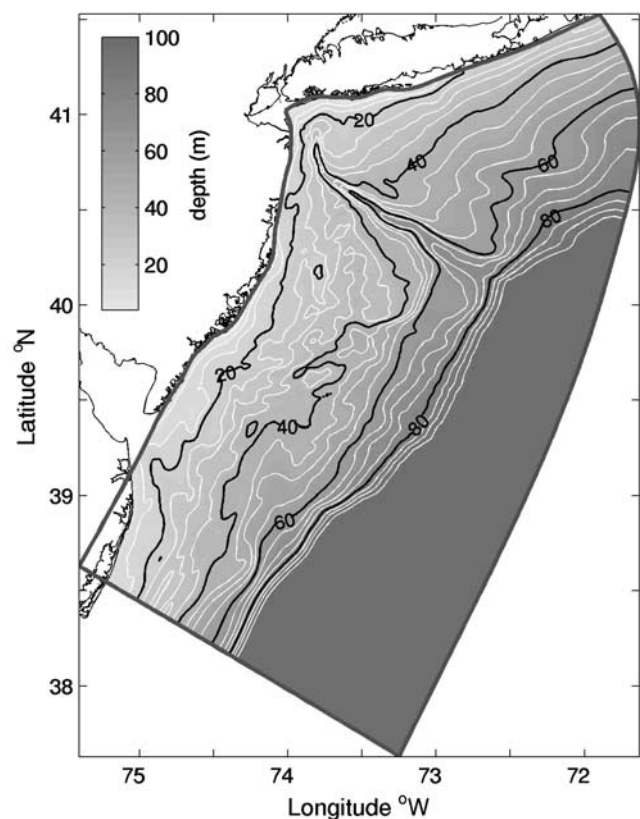


**Figure 2.** ROMS Long-term Ecosystem Observatory (LEO) model grid and bathymetry.

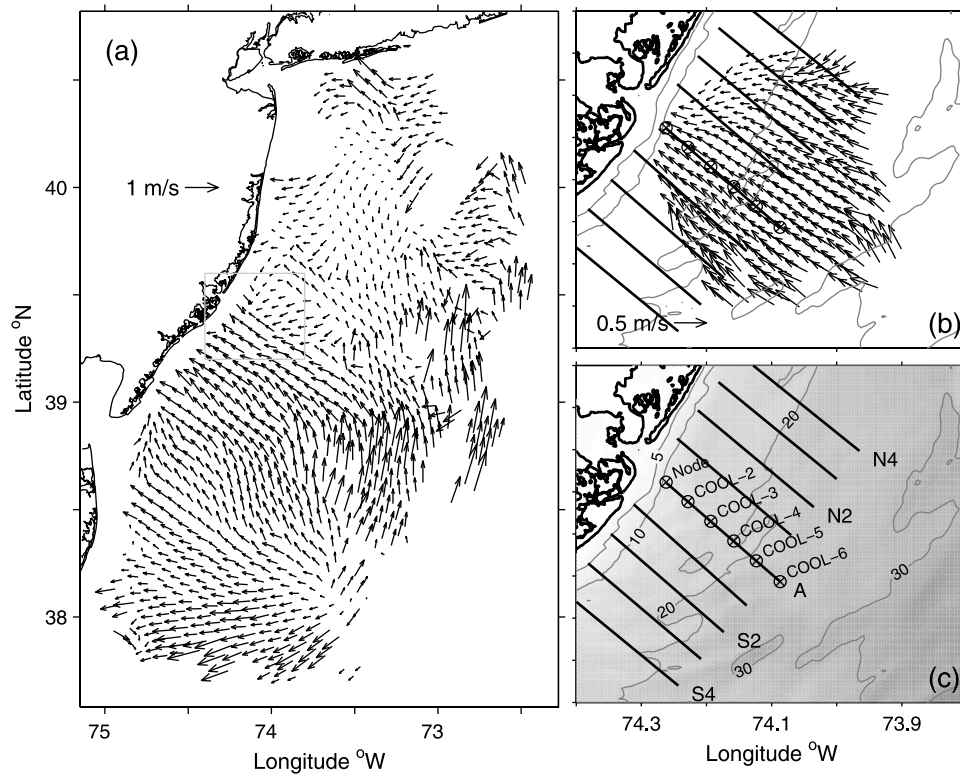


**Figure 3.** (a) Long-range and (b) high-resolution coastal radar (CODAR) surface currents during the downwelling event of 18 July 2001, respectively. (c) Towed-body transect lines occupied by R/V *Mighty Caleta* denoted S4, S2, A, N2, and N4. Conductivity-temperature-depth (CTD) data from approximately four transects could be completed on any day for assimilation in the forecast model. Coastal Ocean Observation Laboratory (COOL)-1 (node) through six thermistor and acoustic Doppler current profiler (ADCP) moorings used for model validation were placed along the A line. Shading and contours show bathymetry. The box in Figure 2a denotes the area depicted in Figures 2b and 2c.

[7] Outflow Orlanski-type radiation conditions [Marchesiello *et al.*, 2001] were applied at the open boundaries to active tracers (temperature and salt) and the nontidal component of velocity. These conditions allow waves generated within the model to exit the domain with few open boundary artifacts, especially given the 1 month duration of the simulations. Given our focus on locally forced inner shelf wind-driven upwelling, open boundary conditions that would impose the weak southwestward mean flow of the outer Mid-Atlantic Bight were not incorporated.

[8] Air-sea fluxes of momentum and heat were computed using standard bulk formulae [Fairall *et al.*, 1996] applied to the modeled sea surface temperature and atmospheric marine boundary values (10 m wind, sea level air temperature, pressure and relative humidity) from two U.S. Navy atmospheric forecast products. These were the operational 27 km resolution West Atlantic region COAMPS forecast [Hodur *et al.*, 2002] (nested within the Navy Operational Global Atmosphere Prediction System (NOGAPS) global forecast), and an experimental 6 km resolution COAMPS forecast further nested within the 27 km domain. A comparison of these forecasts with independent meteorological observations at RUMFS shows that the 6 km resolution COAMPS achieved a high degree of forecast skill during the CPSE period [Bowers *et al.*, 2002]. In the results presented here, 6 km COAMPS data at 30 min intervals were used in all simulations.

[9] During 2001, ROMS forecasts were run with two vertical turbulence closure schemes: the  $k$  profile parameterization (KPP) [Large *et al.*, 1994; Durski *et al.*, 2004], and Mellor-Yamada 2.5 (MY) [Mellor and Yamada, 1982]. Benthic boundary layer dynamics were parameterized according to the wave current interaction model of Keen and Glenn [1995] with an assumed July climatological wave field propagating onshore normal to the shelf break with significant wave period of 10 s and amplitude 0.3 m.

## 2.2. Assimilation Data Sets and Methods

[10] Real-time data were available at LEO during each of the annual Coastal Predictive Skill Experiments from 1998 to 2001. In 2001, the observational network achieved its most comprehensive deployment. Data sets collected included satellite-derived sea surface temperatures, a nested grid of high-frequency radar-derived (CODAR) surface currents from a long-range (LR) regional array and a high-resolution (HR) local array [Kohut *et al.*, 2004], and temperature and salinity profiles from a CTD deployed by undulating shipboard towed-body along a standard set of transects (Figure 3).

[11] Kohut *et al.* [2004] and references therein describe the LEO CODAR system in detail. The CODAR instrument exploits radio wave backscatter from surface gravity waves to measure ocean surface current in the upper meter of the water column in the direction of the radar beam. Radial

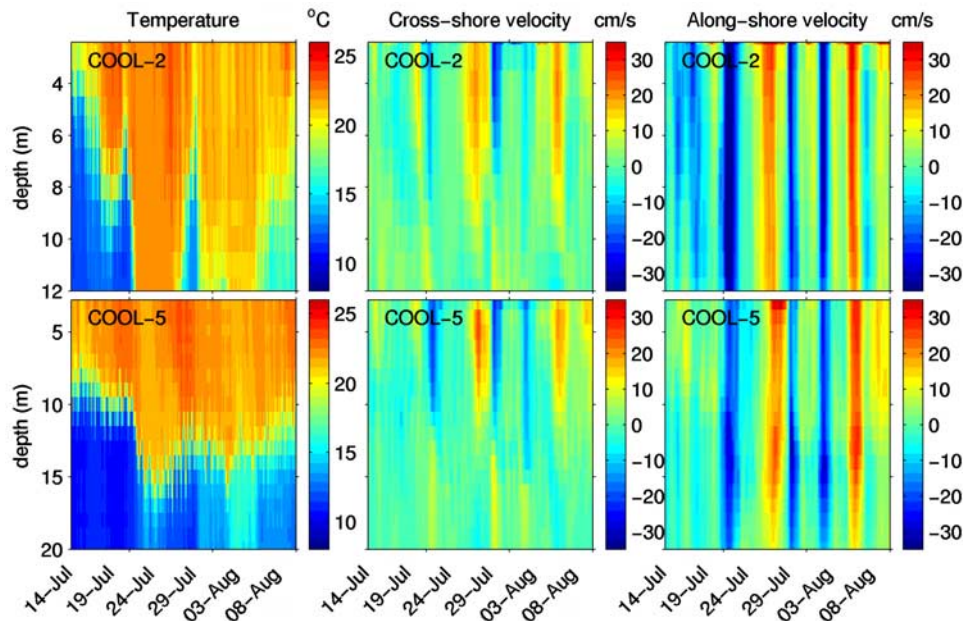


**Figure 4.** Time series of detided temperature and velocity at COOL-2 and COOL-5. Cross-shore velocity is positive toward the southeast. Alongshore velocity is positive toward the northeast.

components of the current from two receiver sites along the New Jersey coast are combined into total surface velocity maps for analysis and assimilation.

[12] At the time of the 2001 CPSE study, the two data assimilation techniques that were available to implement practically in ROMS given the operational constraints of a 3 day forecast cycle were nudging, and simple suboptimal intermittent melding [Dombrowsky and De Mey, 1992]. The temperature and velocity data were assimilated in the form of three-dimensional analyses mapped to the model grid. This mapping step, and the associated forecast and data error covariance estimation procedure, are described in subsequent sections.

[13] In the three years since the 2001 field season tangent linear and adjoint codes [Moore et al., 2004] have been written for ROMS. These codes underpin variational assimilation methods being formulated as part of follow-on projects from the CPSE program, but the results presented here will be confined to the operational intermittent assimilation system available for applications in 2001.

### 2.3. Validation Data Sets

[14] In 2001, the Rutgers Coastal Ocean Observing Laboratory (COOL) augmented the real-time instrumentation by deploying a cross-shelf array of six moorings at 4 km spacing along the central line through the LEO intensive observing area (Figure 3). Each mooring comprised a thermistor string and a bottom-mounted ADCP. Thermistors were placed every 0.3 m in the vertical at COOL-1, and every 1 m at COOL-2 through COOL-5. COOL-1 was deployed alongside the LEO Node ADCP. COOL-6 was a bio-optical mooring [Chang et al., 2002]. These instruments did not telemeter data, and did not enter the data stream used for assimilation in ROMS. They therefore represent a withheld data set suited to evaluating the model skill at forecasting the vertical stratification and across-shelf loca-

tion of upwelling and downwelling fronts and their associated currents.

[15] We describe here the general character of the mooring time series data, and the circulation events they portray, prior to introducing the model skill metrics developed to focus on the essentially two-layer upwelling/downwelling dynamics that represent the principal mode of variability at LEO on timescales of a few to several days.

[16] Time series of temperature and detided cross-shelf and alongshelf velocity are shown in Figure 4 for COOL-2 and COOL-5. Offshore at COOL-5, a persistent sharp thermocline is found between 8 and 16 m depth. Near shore at COOL-2, the two-layer system responds to the winds by alternating between downwelling and upwelling regimes. On three occasions during the observation period, downwelling was sufficiently strong that the downwelling front moved seaward of COOL-2, forming a zone near the coast of weakly stratified warm water. Only for brief periods during this deployment were upwelling winds persistent enough to move the upwelling front seaward of COOL-2, producing the complementary situation of uniform cool waters from surface to seafloor. Low-pass filtered cross-shelf velocities show a pronounced baroclinic response at COOL-5 throughout the deployment, and at COOL-2 when two layers are present. Alongshelf velocities are predominantly barotropic at both sites, with the least vertical variation inshore at COOL-2.

### 3. Operational Forecasting Procedure

[17] During the 2001 CPSE period, ensembles of 3 day ocean forecasts were produced using both high- and low-resolution COAMPS atmospheric forecasts, and both vertical turbulence closure options. The Coastal Ocean Observing Laboratory (COOL) science team evaluated these forecasts qualitatively during twice weekly “briefing

sessions” at RUMFS at which a consensus was formulated on which of the standard towed-body survey lines would yield data of greatest value for initializing the model forecast for the subsequent 3 day cycle, while also meeting the requirements of bio-optical, ecosystem and ocean physics sampling within operational constraints. This typically led to targeting lines that would be upstream of the central mooring line. The real-time forecast system was implemented as follows.

### 3.1. Initial Conditions

[18] In June 2001, a research cruise by the R/V *Endeavor* conducted a survey of the New Jersey Bight region, occupying stations along 7 sections perpendicular to the coast from Sandy Hook to Cape May, out to some 80 km offshore. These stations showed a consistent pattern of typical late spring conditions in this region; namely, an approximately 10-m-deep mixed layer of water near 20°C, laying over cool 10°C water near shore, but cooler 6°C water offshore. These data defined a typical vertical temperature profile indicative of near shore stratification conditions that was used to initialize the model on 1 July 2001. The initial velocity and sea level height were set to zero. At first, the 6 km COAMPS data were unavailable and ROMS was driven with outputs from NOGAPS for 9 days. The temperature solution at 9 July 2001, with sea surface temperature values reset from a 7 day satellite composite, became the starting point for the first ROMS assimilation cycle.

## 3.2. Forecast and Assimilation Cycle

### 3.2.1. Temperature and Salinity

[19] Each 3 day forecast proceeded in the following steps. The preceding forecast cycle was considered an a priori estimate of the ocean state,  $\phi^f$ , where  $\phi$  can be any model variable (temperature, salinity etc.). The difference between  $\phi^f$  and observations  $\phi^{\text{data}}$  gathered during the cycle was mapped to the model grid using optimal interpolation at daily intervals. The mapped adjustment is given by  $\phi' = \mathbf{CA}^{-1}(\phi^{\text{data}} - \phi^f)$  where matrix  $\mathbf{C}$  is the covariance of each model grid point with each observation location and time, and  $\mathbf{A}$  is the covariance of the observations with each other [see, e.g., *McIntosh*, 1990; *Daley*, 1991]. A Gaussian covariance function was assumed with scales of 50 km and 2 days. The ratio of observational error to signal variance that augments the diagonal of  $\mathbf{A}$  was set constant at  $10^{-2}$ . The gridded observations are then  $\phi^o = \phi^f + \phi'$ , and have normalized expected error variance,  $e_o^2$ , given by  $\text{diag}(\mathbf{I} - \mathbf{CA}^{-1}\mathbf{C}^T)$  where  $\mathbf{I}$  is the identity matrix [*McIntosh*, 1990]. In regions of the model domain several covariance length scales distant from any data, the adjustment  $\phi' \rightarrow 0$ ; the model state ( $\phi^f$ ) is retained and  $e_o^2 \rightarrow 1$ . Close to observation locations, the data supplant the model forecast in proportion to the model-observation mismatch and the chosen covariance scales;  $e_o^2$  is small. The model was then restarted from the beginning of the previous forecast, with the daily optimally interpolated gridded data fields for temperature and salinity assimilated over 3 days by one of two methods: “nudging” or “melding.”

[20] In the case of nudging, the model solution is pushed toward the mapped data on every time step with a right-hand-side term proportional to  $\lambda(\phi^o - \phi^f)$ , where  $\lambda =$

$(1 - e_o^2)/\tau_n$  is a nudging inverse timescale  $1/\tau_n$  down weighted by the expected error. The timescale adopted was  $\tau_n = 7$  days for both temperature and salinity.

[21] The melding assimilation follows the method of *Dombrowsky and De Mey* [1992], which, in common with optimal interpolation, is founded on Gauss-Markov theory. At the times corresponding to the  $\phi^o$  maps, a weighted sum of observations and forecast is computed as  $\phi^a = \mu\phi^o + (1 - \mu)\phi^f$ . The weights given by  $\mu = (e_f^2 - \gamma e_o e_o^2)/(e_o^2 + e_f^2 - 2\gamma e_o e_o^2)$  are optimal in the sense that the “analysis” estimate  $\phi^a$  has the minimum expected mean squared error for the assumed error variance of observations and forecast. The model is reinitialized with  $\phi^a$  and the integration proceeds. We take  $\gamma = 0.01$  for the correlation between model and observations. (See *Dombrowsky and De Mey* [1992] for a discussion of the role of this parameter.) At each melding reinitialization, the forecast error is reset to the analysis error,  $e_a^2 = e_f^2 e_o^2 (1 - \gamma)/(e_o^2 + e_f^2 - 2\gamma e_o e_o^2)$ . In the absence of any experience evaluating the forecast skill of the model at the time of the 2001 CPSE, we assumed that the model error,  $e_f^2$ , grew exponentially with a timescale of 10 days.

[22] At the conclusion of the assimilation period (whether it be by nudging or melding), the previous forecast has been adjusted to reflect the observations acquired, and this new hindcast state becomes the initial condition for the next ocean forecast cycle forced with the new 3 day atmospheric prediction.

### 3.2.2. Coastal Radar (CODAR) Surface Currents

[23] Both the nudging and melding assimilation approaches can equally well be applied to CODAR observations of surface velocity. However, in practice, such simple schemes require that surface current observations should be projected vertically to other depths if at all possible. CODAR observations could be assimilated into only the surfacemost level of the model by nudging or melding, but this risks introducing significant vertical shear in the horizontal velocity which the model physics interprets as demanding enhanced vertical mixing due to a diminished Richardson number.

[24] In July 2001, long-range (LR) CODAR data became available shortly before commencing operational forecasting on 11 July, whereas the high-resolution (HR) CODAR system had been operating for 2 years. A decision was made at the time to use 3 hourly averaged LR-CODAR and 1 hourly averaged HR-CODAR velocities (e.g., Figure 3), extrapolated vertically using a simple exponential function, to generate depth-varying horizontal velocity analyses for assimilation in ROMS. This simplistic CODAR processing was subsequently found to be inadequate in several respects, adversely impacting the forecast skill. A modified subsurface projection scheme based on correlations between CODAR and the moored ADCP data has been formulated. We have elected to present model results here that use this alternative scheme, even though this was not the data processing procedure used operationally in 2001. To do otherwise would unfairly cast the CODAR data as being of little value, whereas we show in the next section that even a straightforward statistically based vertical extrapolation of surface CODAR observations has significant skill at estimating subsurface velocity in the LEO region, and CODAR data offer considerable promise for incorporation into coastal ocean data assimilation forecast systems.

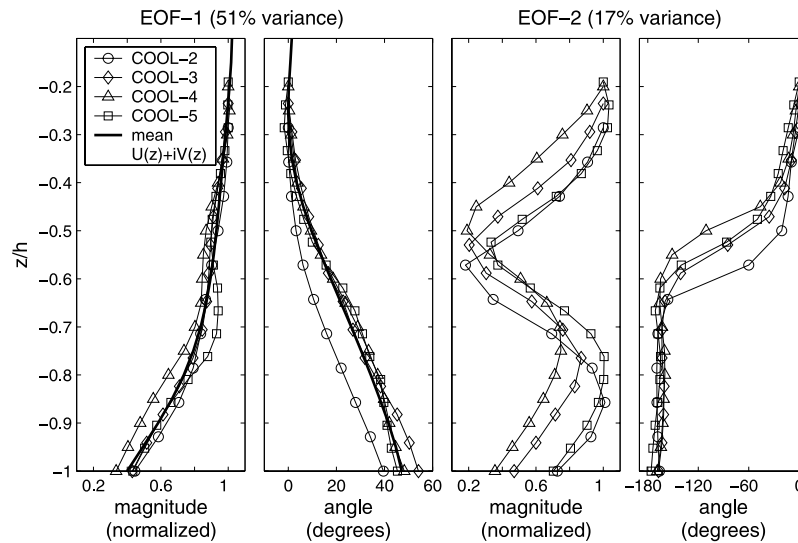


**Figure 5.** Empirical orthogonal functions (EOFs) of velocity variability from four Coastal Ocean Observation Laboratory (COOL) ADCPs deployed during July 2001 LEO Coastal Predictive Skill Experiment.

[25] Empirical orthogonal functions (EOF) of velocity variability at the ADCP moorings COOL-2 through 5 all show similar vertical structure (Figure 5). For the first EOF (typically 51% of variance), the decreasing magnitude and the rotation of flow direction with depth are consistent with a bottom friction dominated boundary layer [Munchow and Chant, 2000]. The second EOF shows a phase difference of  $180^\circ$  between surface and bottom in accordance with a simple two-layer upwelling or downwelling response. Regression fits of the CODAR surface velocity to the EOF-1 amplitude time series also give similar coefficients at all ADCP sites, with a mean value of  $0.65 \exp(-i 9.7\pi/180)$  (Table 1). The common pattern across all moorings allows us to hypothesize a consistent relationship predicting the complex velocity at any depth solely from CODAR and the EOF-1 structure:

$$u(z) + iv(z) = c_u U^*(z)(u + iv)_{\text{CODAR}}, \quad (1)$$

where  $c_u$  is the mean correlation coefficient (Table 1) and  $U^*(z)$  is the mean EOF-1 structure (heavy line in Figure 5).

[26] To illustrate the skill of this projection scheme, Figure 6 compares the observed ADCP velocity at COOL-5 to the estimate based solely on CODAR projected with the regression relation given above. The error is typically much less than the variability, even near the seafloor.

[27] In practice, we use equation (1) to produce a three-dimensionally gridded horizontal velocity data set (i.e., for  $\phi^\circ$  above corresponding to velocity components  $u$  and  $v$ ) after first interpolating CODAR velocities to the model horizontal grid points. To complete this formulation for the purposes of data assimilation, the expected error of the inferred subsurface velocity components is required to define  $e_o^2$ . We estimate this from the mean squared error of the projected velocity (equation (1)) compared to that observed by ADCP, as a function of depth (Figures 6c and 7). When normalized by the signal variance, surface

values near 0.2 indicate that CODAR captures 80% of the velocity variability. Near the seafloor, the expected skill of the subsurface projection is still significant but falls to about 40%.

## 4. Forecast System Results

### 4.1. Bottom Temperatures

[28] Owing to the strong stratification that occurs at LEO during summer (Figure 4), the cross-shore movement of waters in response to wind forcing can be seen clearly in a Hovmoeller (distance-time) diagram of the bottom temperature along the COOL mooring line (Figure 8a). During downwelling, the thermocline intersects the seafloor and warm waters spread seaward, whereas upwelling is characterized by the return shoreward of cooler bottom waters. A distinct thermocline front persists throughout these transitions.

[29] Figures 8b and 8c shows the corresponding modeled bottom temperatures when the forecast system is run without assimilation (henceforth denoted experiment 0), and with towed-body CTD data included by melding (experiment 1a). CODAR data were not used in these cases, and the vertical turbulence closure was KPP. Qualitatively, both

**Table 1.** Regression Coefficients for Coastal Radar (CODAR) Versus Acoustic Doppler Current Profiler (ADCP) Empirical Orthogonal Function (EOF)-1 Velocity<sup>a</sup>

ADCP Site	ADCP EOF-1 Versus CODAR Regression Coefficient, $c_u$	
	Magnitude	Angle, deg
COOL-2	0.69	-9.6
COOL-3	0.65	-14.0
COOL-4	0.70	-3.2
COOL-5	0.65	-11.9
Mean	0.67	-9.7

<sup>a</sup>Negative angles indicate the surface velocity is to the right of CODAR.

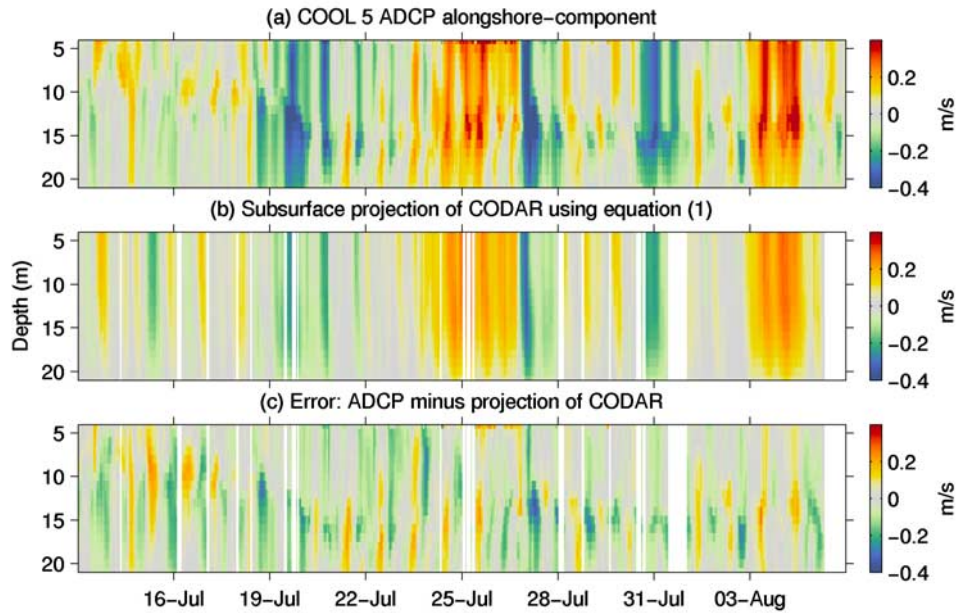


**Figure 6.** (a) Alongshore component of current observed by COOL-5 ADCP as a function of depth and time. (b) Alongshore current at COOL-5 estimated using surface current from HR-CODAR and equation (1). (c) Error of the vertical projection scheme of Figure 5a minus Figure 5b.

forecasts track the observed bottom temperature well, but the result is better with data assimilation. Melding events, when the model state is essentially reset to match the available observations, produce abrupt changes in the solution in several instances. The melding steps occur at irregular intervals because of the weather dependence of operating a towed-body from the small coastal vessel R/V

*Mighty Caleta*. Nevertheless, even during the protracted data gap from 25 to 28 July, the solution with assimilation performed better than that without. With assimilation, the model correctly cooled due to upwelling whereas without assimilation the solution is too warm. Observed cooling events on 31 July and 5 August are similarly forecast better when the model assimilates CTD data.

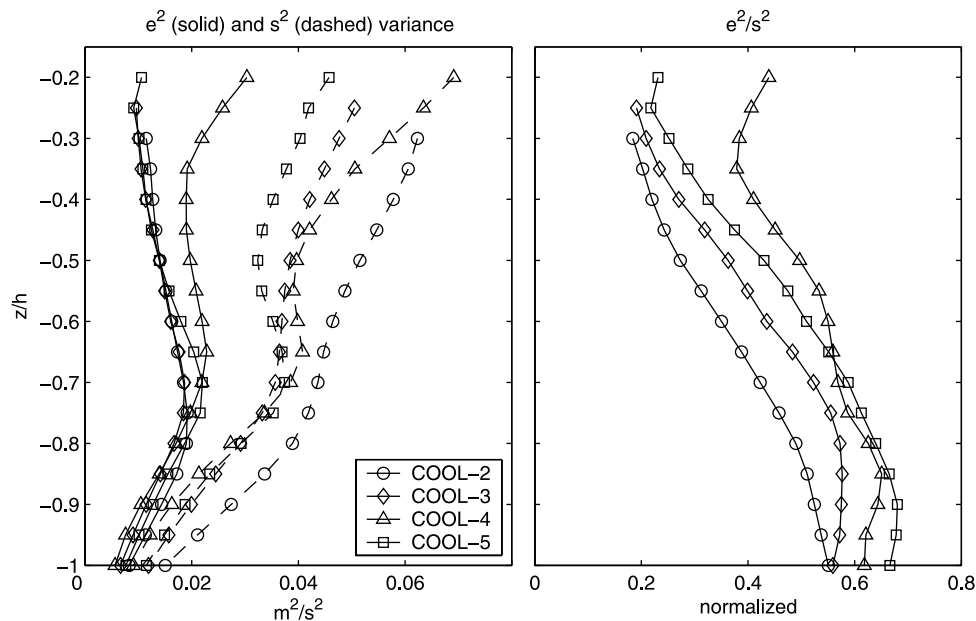


**Figure 7.** (left) Time-averaged error variance of subsurface projection (Figure c) at the COOL-2 through COOL-5 mooring sites. (right) Error variance normalized by signal variance. An average of the four  $e^2/s^2$  curves was used to define the normalized data error variance  $e_o^2$  used in the assimilation schemes.

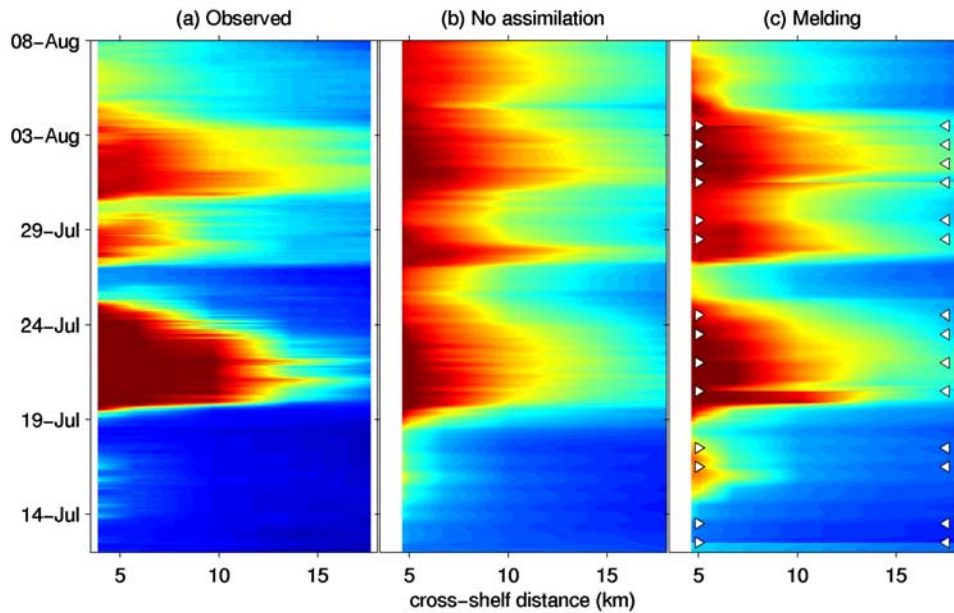


**Figure 8.** Seafloor temperature along the central mooring line as a function of time. (a) Observed at moorings 2–5. Forecast using (b) no assimilation and (c) intermittent melding to assimilate towed-body CTD observations. No CODAR data were used in these cases. The marks in Figure 7c indicate times at which sufficient data were available to produce a useful gridded data set for assimilation.

[30] The overall correspondence between observations and experiment 0 suggests that the ocean model has significant intrinsic skill, while the comparison to experiment 1a indicates that data assimilation can improve the forecast. These qualitative results are explored further in the next section.

#### 4.2. Temperature and Transport Validation Metrics

[31] To introduce rigor into the comparison of mooring observations and forecasts, a set of quantitative model evaluation metrics were developed based on a two-layer interpretation of the circulation. The boundary between the two layers was deemed to be where the vertical temperature gradient is a maximum. With this definition, surface, average upper-layer, and average lower-layer temperatures can be calculated for both mooring and model profiles. We also compute the difference in cross-shore transport integrated over each layer which we denote the “baroclinic transport” associated with the two-layer circulation. To complete the metric set, we calculate the depth integrated alongshore transport as an indicator of the strength of the coastal jet associated with upwelling and downwelling. Time series of these metrics from the mooring data at COOL-3 are compared to experiments 0, 1a and 1b (as for experiment 1a but with MY25 turbulence closure) in Figure 9. The squared coherence of experiments 0 and 1a with the data is plotted in Figure 10.

[32] The modeled thermocline depth is initially too great and surface temperatures are too warm, indicating an imperfect initial condition. In all model configurations, the thermocline depth comparison improves by 16 July, but sea surface temperatures for experiment 1a do not approach agreement until the downwelling event of 19 July begins. Experiment 1b never captures SST well.

[33] Despite the cool bias in forecast upper-layer temperature that lingers from the poor initial condition, SST variability is coherent with observations across all frequencies for both experiment 0 and 1a (Figure 10). This likely results from the considerable skill in the 6 km resolution COAMPS atmospheric forecast being carried through to the air-sea heat fluxes that drive the high-frequency variability that dominates the variance in surface temperature. Interestingly, the model with assimilation generally produces SST variability that is less coherent with observations. This is probably due to modeled diurnal and other high-frequency temperature variability close to the sea surface being upset by melding with 2 day average (the optimal interpolation covariance timescale) towed-body CTD data. In this situation, the expected error  $e_o^2$  of the gridded CTD data is effectively underestimated relative to the expected error  $e_f^2$  of the model forecast, thereby giving the surface temperature observations undue weight ( $\mu$ ) in the melding steps. This interpretation is supported by the result that the upper-layer average temperature metric does show improved coherence when data are assimilated, which suggests that by considering more of the water depth than that affected directly by diurnal heating, the relative magnitude of data and model errors is better estimated and the intermittent melding approach achieves a useful outcome.

[34] Lower-layer temperatures agree better for experiment 1a than 1b, except during the strong downwelling event when experiment 1a sees the return of the thermocline on 21 July while in reality the COOL-3 site is flooded with nearly isothermal warm waters for four days. Inspection of Figure 8 shows that in experiment 1a the across-shore movement of the foot of the downwelling front barely reaches the COOL-3 location (11.7 km from shore) on 20 July. With the exception of the thermocline depth during

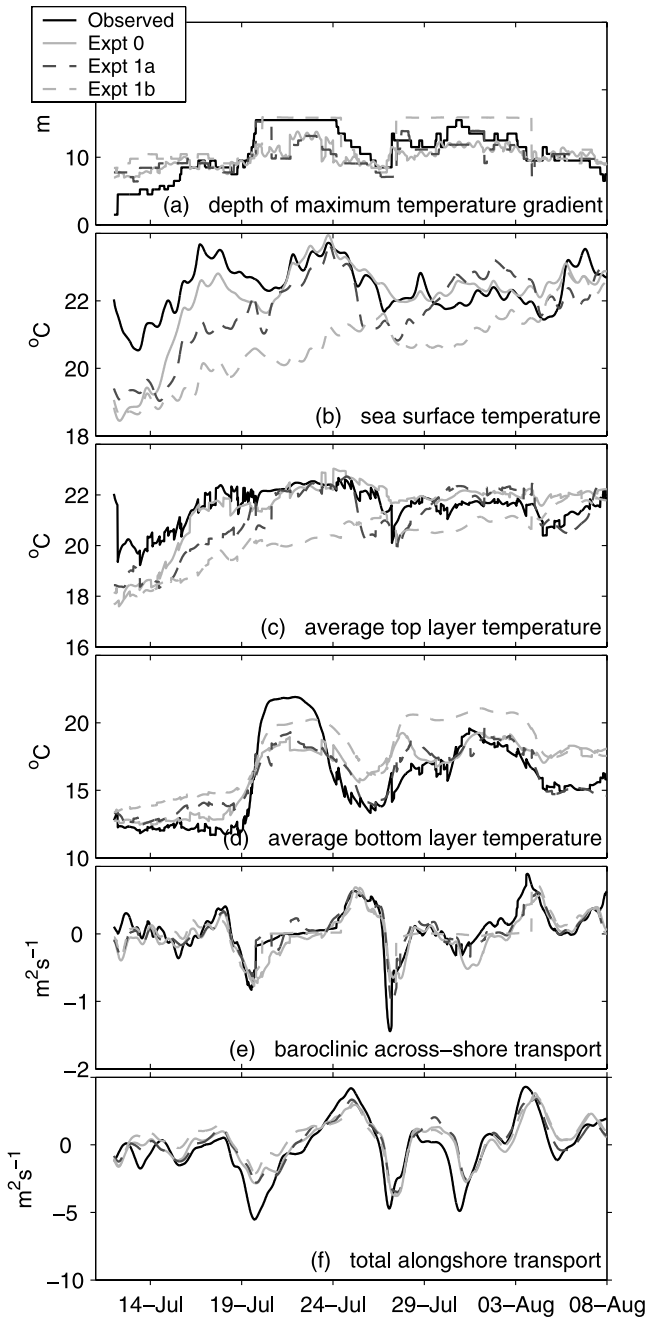


**Figure 9.** Time series of observed and forecast two-layer metrics at the COOL-3 mooring site. Forecasts shown are with no assimilation (experiment 0) and temperature assimilation with KPP (experiment 1a) and MY25 (experiment 1b) vertical mixing. (a) Depth of maximum temperature gradient. (b) Sea surface temperature. (c) Average upper-layer temperature. (d) Average lower-layer temperature. (e) Baroclinic upper-layer across-shore transport (positive offshore). (f) Depth-integrated alongshore transport.

the 19–24 July downwelling, the MY25 turbulence scheme shows poorer agreement with data than KPP, and we will focus on the KPP closure in subsequent analysis of the forecast system performance.

[35] The thermocline depth, defined as where  $\partial T/\partial z$  is a maximum, can be discontinuous in time and so leads to some noisiness in the temperature metrics. (Since the thermocline depth is not formally differentiable in time and can be multivalued, it is omitted from the coherence plots.) However, vertical shear in the cross-shore circulation leads to weak velocities at the layer interface so the cross-

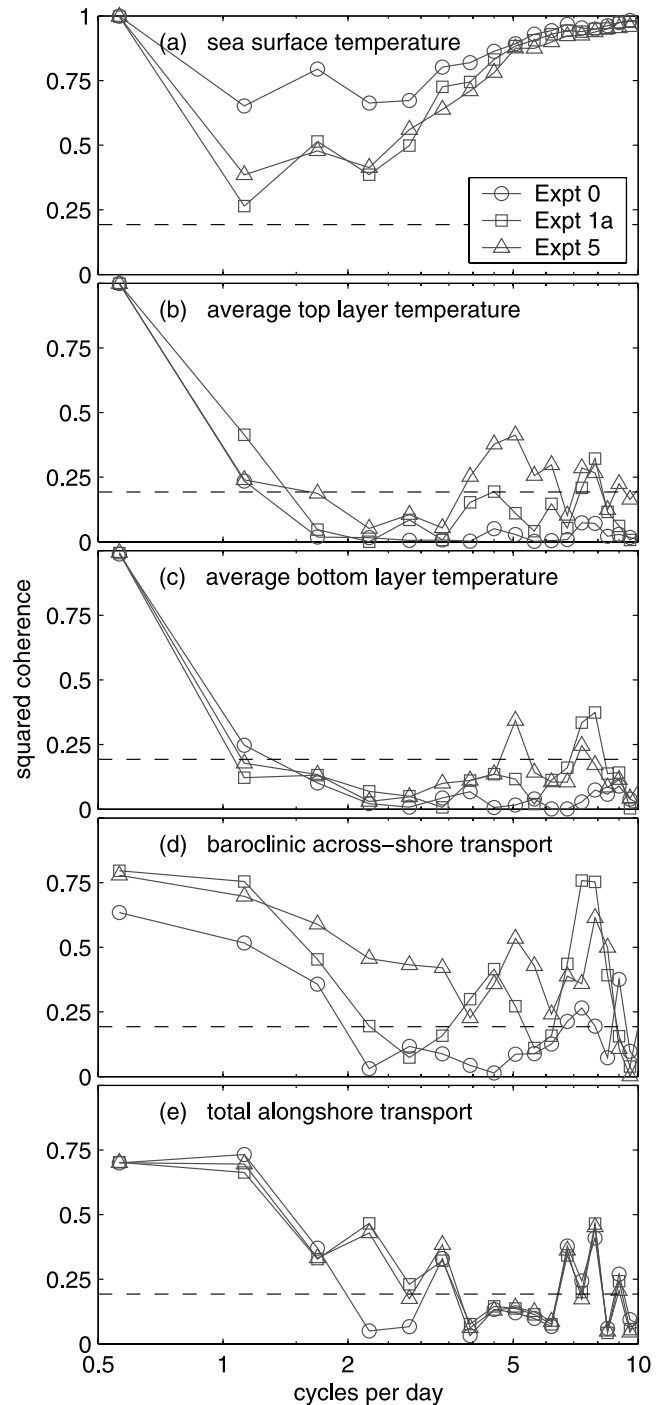


**Figure 10.** Squared coherence of observed metrics with experiment 0 (no assimilation), experiment 1a (assimilation of towed CTD), and experiment 5 (assimilation of towed CTD and HR-CODAR) at COOL-3 mooring site. The dashed line shows the 95% significance limit.

**Table 2.** Summary of Hindcast Experiments<sup>a</sup>

Experiment	CODAR Data Used	CODAR Assimilation Method	CTD Assimilation Method
0	...	...	...
1a	...	...	melding
2	HR + LR	nudging	nudging
3	HR + LR	nudging	melding
4	HR + LR	melding	melding
5	HR	melding	melding
6	HR	nudging	melding
7	...	...	nudging

<sup>a</sup>HR denotes high-resolution CODAR data only, and HR + LR denotes that long-range CODAR was also included. CTD refers to subsurface gridded temperature and salinity observations made from the towed-body profiler.

shore baroclinic transport is less susceptible to uncertainty in the interface location, and much less noisy. Figure 9 shows that both cross-shore and alongshore transports agree well from the very beginning of the forecast, suggesting the essential features of the momentum balance have been modeled well by the forecast system. The transport metrics were found to be largely insensitive to the choice of vertical turbulence closure.

## 5. Data Assimilation System Sensitivity

[36] The forecast system comprises multiple data sets (temperature, HR and LR CODAR) and assimilation options (melding and nudging), and prompts the question: Does a certain combination of data and methods give consistently superior performance as measured by the model skill metrics? To address this, we conducted a suite of hindcast simulations that systematically varied the model configuration options to consider assimilation of towed-body CTD observations by melding (experiments 1a, 3, 4, 5, 6) or nudging (experiments 2, 7), assimilation of HR-CODAR only (experiments 5, 6), or HR and LR-CODAR combined (experiments 2, 3, 4), with the CODAR assimilation method being melding (experiments 4, 5), nudging (experiments 2, 3, 6) or no CODAR assimilation at all (experiments 1a, 7). These options are summarized in Table 2.

[37] The summary model skill statistic we present is the mean squared error (MSE) [e.g., Oke *et al.*, 2002a] of the time series of modeled ( $m_i$ ) and observed ( $o_i$ ) metrics:

$$\text{MSE} = \frac{1}{n} \sum_{i=1}^n (m_i - o_i)^2,$$

where  $n$  is the number of values in the hindcast time interval. The MSE for the layer average temperature and transport metrics at each COOL mooring, and the average over all moorings for each experiment, are given in Table 3. The lowest MSE for each metric is highlighted. No single configuration performs best for all metrics, though some consistent patterns emerge.

[38] As expected from the discussion above, experiment 0 (no assimilation) scores best on average over all moorings for the simulation of upper-layer temperature. Experiment 5 assimilates HR-CODAR and CTD data by melding, scoring

best in the average over all moorings in terms of lower-layer temperature and alongshore transport (equal with experiment 0), and second best on the other two metrics. Compared to experiment 1a, experiment 5 has lower average MSE for all four metrics indicating that the assimilation of HR-CODAR by melding consistently improves performance. Overall, we consider experiment 5 the best configuration.

[39] Results for the SST metric are not tabulated but tell essentially the same story as upper-layer temperature (ULT). The three lowest mean MSE of 0.020, 0.025 and 0.03 for experiments 7, 0 and 1a, respectively, are virtually equal. Experiment 5 is next (MSE = 0.07) with the other configurations in the same order of increasing MSE as for ULT. As noted above, SST variability is coherent across all frequencies, but the MSE metric for SST is dominated in most cases by a low-frequency cool bias.

[40] While the merits of melding over nudging are clear for HR-CODAR (the MSE for all metrics in experiment 5 is

**Table 3.** Mean Squared Error (MSE) of the Layer Temperature and Transport Metrics for the Data Assimilation Sensitivity Experiments<sup>a</sup>

Experiment	Mooring				Mean
	2	3	4	5	
<i>Lower-Layer Temperature, °C<sup>2</sup></i>					
0	1.02	0.43	0.93	0.52	0.73
1a	0.32	0.03	0.51	0.54	0.35
2	0.64	0.16	0.70	0.37	0.47
3	0.26	0.08	0.67	0.73	0.43
4	1.27	2.11	3.54	3.34	2.57
5	0.15	0.06	0.40	0.27	<b>0.22</b>
6	0.60	0.29	0.85	0.71	0.61
7	0.84	0.24	0.70	0.48	0.57
<i>Upper-Layer Temperature, °C<sup>2</sup></i>					
0	0.01	0.001	0.004	0.001	<b>0.004</b>
1a	0.15	0.28	0.001	0.05	0.12
2	0.03	0	0.04	0.007	0.02
3	0.06	0.05	0.001	0.001	0.03
4	0.76	0.87	0.63	0.70	0.74
5	0.02	0.02	0.02	0.02	0.02
6	0.42	0.52	0.41	0.51	0.46
7	0.04	0	0.02	0.001	0.01
<i>Alongshore Barotropic Transport, m<sup>4</sup> s<sup>-2</sup></i>					
0	0	0.14	0.49	0.19	<b>0.20</b>
1a	0.015	0.15	0.74	0.48	0.34
2	0.027	0.30	0.64	0.28	0.31
3	0.015	0.43	0.87	0.44	0.44
4	0.005	0.16	0.62	0.24	0.26
5	0.018	0.22	0.43	0.13	<b>0.20</b>
6	0.044	0.39	0.76	0.31	0.37
7	0.001	0.17	0.66	0.28	0.28
<i>Across-Shore Baroclinic Transport, 10<sup>-3</sup> m<sup>4</sup> s<sup>-2</sup></i>					
0	0.82	6.0	4.0	2.2	3.2
1a	0	0.05	12.2	0.18	<b>2.1</b>
2	0.18	3.7	2.2	4.8	3.7
3	0.25	2.8	2.5	5.8	2.8
4	0.37	0.8	11.8	0.42	3.4
5	0.15	4.0	2.9	4.1	2.8
6	0.27	3.4	2.2	9.2	3.7
7	0.31	3.8	5.2	3.7	3.3

<sup>a</sup>Results are tabulated for each mooring and for the mean over four moorings. The lowest MSE in each column is in boldface. See Table 2 for experiment options.

less than in experiment 6), the better method for CTD data assimilation is not readily evident. If we eliminate the possibly confounding role of simultaneously assimilating CODAR data, so compare only experiments 0, 1a and 7, we see that both methods improve the forecast skill of the bottom layer temperature, with melding again performing best. Neither method makes an appreciable difference to the across-shore transport. The alongshore transport loses skill when temperature data only are assimilated, but with this loss being less pronounced in the case of nudging.

[41] The coherence of observed and modeled metrics for experiments 1a and 5 are compared in Figure 10. Assimilation of temperature data significantly increases the coherence of cross-shore transport at low frequencies compared to experiment 0. The introduction of HR-CODAR assimilation further expands the coherence to all resolved frequencies. For alongshore transport, assimilation increases the maximum coherent frequency from 2 cycles  $d^{-1}$  to 3.4 cycles  $d^{-1}$  (7 hour period). Some coherence in the upper-layer temperature variability is also recovered in experiment 5 at around 4 to 6 hour periods. Two hours would be the shortest period resolvable by the hourly assimilation interval for HR-CODAR, so there is some potential utility in assimilating such high-frequency data.

[42] The addition of long-range CODAR, however, does not bring further overall improvement. The MSE in alongshore transport decreases in experiments 3 and 4 compared to experiment 1a, but the lower-layer temperature error increases. Assimilation of LR-CODAR by melding, in particular, gives very poor performance for the temperature metrics. Since the lower-layer temperature is controlled primarily by advection associated with the two-layer circulation, the inclusion of LR-CODAR must upset the modeled transport pathway for the lower layer and cause water to be drawn from a source region with different temperatures. This suggests our vertical projection of CODAR velocities to the lower layer is not valid beyond the immediate environs of the relatively shallow LEO region. This is hardly surprising because the projection uses the vertical profile of the first EOF of the ADCP data, which is orthogonal to the second EOF that exhibits a two-layer pattern (Figure 5b). Formally speaking, the error is not so much with the projection scheme itself but more that the expected error of the projection is underestimated and CODAR is given undue weight in deep water. This result is not inconsistent with the reduced alongshore transport error because EOF-1 captures most of the depth-integrated flow, and the depth integral of EOF-2 is almost zero.

[43] However, how can it be that our assimilation scheme adds skill for HR-CODAR if it uses the same, potentially flawed, vertical projection? There are two considerations here.

[44] The first is that near the coast in an approximately two-dimensional upwelling circulation the flow is predominantly parallel to shore (the coastal jet) and alongshore temperature gradients dominate the lateral divergence of heat. This is especially so inshore of the front. Velocities in the LEO region typically persist at about  $10 \text{ cm s}^{-1}$  for the duration of an individual upwelling or downwelling event. Over the 3 day forecast cycle, this speed would draw water from 25 km away, which is roughly the coverage of the HR-CODAR but also the range from the COOL mooring line to

the furthest towed-body CTD transects (Figure 3). Within the scope of the HR-CODAR then, there are CTD data available for assimilation so that the temperature field is adjusted to agree with observations. Accordingly, the dominant features of the temperature and velocity, and therefore lateral heat advection, are usefully constrained by the combined data assimilation.

[45] Secondly, beyond the nearshore region of an upwelling front and coastal jet at LEO, *Chant et al.* [2004] find the circulation is strongly three-dimensional, contributing significantly to the cross-shore divergence of heat, while *Kohut et al.* [2004] emphasize that stratification decreases the vertical correlation of currents. In this region of the forecast model, surface LR-CODAR observations were weakly, but erroneously, projected to the lower layer, which will incline the model to draw upwelled water from the wrong region.

[46] Furthermore, in the CPSE program this region was largely outside the scope of CTD sampling by the R/V *Mighty Caleta*, and any departures of the model temperature from reality were unconstrained by observations. In this situation, even a perfect velocity field achieved with more skillful assimilation of LR-CODAR would be prone to errors if there is no mechanism to correct a far field bias in the temperature.

[47] We conclude, therefore, that beyond the central LEO observing area an inappropriate vertical projection of CODAR and the lack of in situ observations to constrain the model temperature field combine to negatively impact the simulated heat transport and degrade the temperature metrics when LR-CODAR was used. However, this is not to say that CODAR data are not useful for constraining simulated currents in this model. Our statistical vertical projection was determined locally from ADCP data in the central LEO region, and in this region the assimilation of HR-CODAR added skill. Evidently, a different projection is required elsewhere in the LEO model domain.

[48] Some alternative methods have been tested by other investigators. *Paduan and Shulman* [2004] used with success a vertical projection based on Ekman theory to assimilate CODAR data in a model of Monterey Canyon, a deep region beyond the shelf break that, unlike the New Jersey Bight, does not have overlapping surface and bottom boundary layers. In a model of subtidal frequency current variability in water depths of 50 to 200 m on the Oregon shelf, *Oke et al.* [2002b] used inhomogeneous anisotropic covariance patterns derived from an ensemble of forward model runs to distribute corrections horizontally and vertically throughout the model domain using the Physical-space Statistical Analysis System (PSAS) of *Cohn et al.* [1998]. This approach could be applied in the LEO setting if it proved valid to assume the covariance patterns are stationary in time, and provided the method could be adapted to accommodate higher-frequency tidal and inertial variability on a broad, shallow shelf. A further alternative is the four-dimensional variational method [e.g., *Moore et al.*, 2004] which uses the adjoint of the forecast model to determine patterns of space and time covariance.

## 6. Forecast System Design

[49] The melding and nudging approaches adjust the model state only at times and places coinciding with

available data, with some extrapolation embodied in (1) the covariance scales adopted for the gridding of temperature and salinity data ( $\sim 50$  km) and (2) the vertical projection of CODAR. In this strongly advection-dominated flow regime, the transport of water from beyond the scope of the observational network (25 km) in a forecast cycle (3 days) frequently occurs. Unless these waters have some memory from earlier cycles (i.e., they previously passed through the observational area and were subject to nudging or melding), their properties are unconstrained by assimilation and their temperature and salinity will depend on initial and boundary conditions, surface fluxes, and the skill of the forecast model. It was shown that the forecast model has useful intrinsic skill, but that the initial conditions were imperfect. Without validation data beyond the central mooring line, it is difficult to say whether the modeled circulation achieves the skill demanded for analysis of ecosystem and bio-optical properties that respond to longer timescales and space scales associated with transport from beyond the LEO intensive observing region.

[50] To meet these demands, the in situ sampling program would need to extend beyond the central LEO region to a range that fully encompasses the water masses that are likely to enter the region of interest on the subsequent forecast cycle. This would be some 60 km at least from the COOL mooring sites, and beyond the adaptive sampling capabilities (range and weather dependence) of a single small coastal vessel. Fleets of autonomous underwater gliders of the type prototyped during 1999–2001 CPSEs are more suited to the task of gathering the broad spatial scale in situ temperature and salinity data required for such a coastal predictive system. Glider fleets are less weather-dependent, able to cover a greater spatial domain, yet profile through the vertical stratification and across horizontal fronts.

## 7. Conclusions

[51] The LEO Coastal Predictive Skill Experiments provided a well-sampled ocean environment in which to evaluate a coastal ocean forecast system for a strongly stratified, predominantly two-layer, system with alongshore barotropic and cross-shore baroclinic transport driven by local winds.

[52] The forecast system developed employed the circulation model ROMS in conjunction with simple data assimilation methods that utilized surface current observations from HF radar (CODAR) systems and real-time in situ temperature and salinity data from a towed-body CTD. Forecast evaluation was in terms of a set of metric time series designed to characterize the predominant aspects of the two-layer circulation: upper- and lower-layer average temperatures, alongshore barotropic transport, and baroclinic cross-shelf exchange transport.

[53] The forecast model, without assimilation, had considerable skill at reproducing temperature and current variability observed by a cross-shelf array of validation moorings at the center of the LEO intensive observing area, but this skill could be further improved with data assimilation. Of the data assimilation configurations tested, that with the greatest skill used intermittent melding [Dombrowsky and De Mey, 1992] of temperature and high-resolution

CODAR. Melding clearly performed best for assimilating HR-CODAR, but it was less clear whether nudging or melding is preferred for incorporating subsurface temperature and salinity data acquired by towed-body CTD.

[54] Forecast SST was coherent with observations at all frequencies. Upper- and lower-layer average temperatures were coherent at frequencies up to  $1.5$  cycles  $d^{-1}$ . Transport time series were forecast better, with alongshore transport typically being coherent up to  $3$  cycles  $d^{-1}$ . The introduction of HR-CODAR greatly extended the coherence of forecast cross-shore baroclinic transport.

[55] It is our conjecture that melding, which reinitializes the model state at intermittent intervals, allows the model to pursue its own trajectory until the next data assimilation step; this evolution is typically quite skillful (as evidenced by the model skill without assimilation) and is aided by the accuracy of forcing data from the 6 km COAMPS atmospheric forecast. Assimilation by nudging, on the other hand, can unnaturally constrain the model evolution during the forecast interval, denying the model the opportunity to respond accurately to the forcing. This is especially so if the observational system is unable to return data at sufficiently frequent time intervals.

[56] Some aspects of the observational network were found to be limiting to forecast skill. Imperfect initial conditions inaccurately set the initial thermocline depth and upper-layer temperature. However, after a week of forecasting, memory of this initial error was erased and the temperature metric errors reduced. The transport metrics suffered no such initial error. This is consistent with the dominant features of the mass transport being cross-shore transport set by Ekman dynamics that in turn sets up a pressure gradient that balances an alongshore current (coastal jet). This process is not sensitive to stratification, and is established rapidly by the wind. Arguably then, the two-layer transport metrics are not particularly discriminating validation criteria for the three-dimensional flow response, though the temperature metrics certainly are.

[57] Our methods were unable to achieve an increase in forecast skill through the assimilation of long-range CODAR data. We attribute this to an inaccurate extrapolation of the surface current observations to the rest of the water column in areas of the model domain beyond the central LEO region. This projection is required for the melding and nudging assimilation approaches because the techniques themselves do not adaptively determine spatial or temporal covariance of the data. To assimilate CODAR only at the surface would produce dynamically imbalanced vertical shear. More advanced methods such as four-dimensional variational assimilation presently being developed for ROMS [Moore *et al.*, 2004], or an adaptation to shallow waters of the PSAS method used by Oke *et al.* [2002b], have the potential to overcome this limitation. Given the significant intrinsic skill of the LEO model, future improvements to the assimilation method should enable skilful use of CODAR in further hindcast studies of the data gathered during the LEO Coastal Predictive Skill Experiments.

[58] **Acknowledgments.** The LEO Coastal Predictive Skill Experiments, CODAR development, and ocean modeling efforts were supported by Office of Naval Research grants N00014-97-1-0797 and N00014-00-1-0724. Data used were also acquired with the support of the ONR funded HyCODE program (N00014-99-1-0196) and the National Ocean Partner-

ship Program (N00014-97-1-0797). The ROMS model development is funded by ONR grant N00014-1-0227. Computational resources were provided by the DOD High Performance Computing Modernization Program.

## References

- Bowers, L., S. Glenn, R. Cermak, K. Hedstrom, J. Doyle, and S. Wang (2002), A comparison of the operational and experimental COAMPS meteorological forecasts at LEO during the 2001 HYCODE experiment, *Eos Trans. AGU*, 83(4), Ocean Sci. Meet. Suppl., Abstract OS25E-78.
- Chang, G. C., T. D. Dickey, O. Schofield, A. D. Weidemann, E. Boss, M. A. Moline, and S. M. Glenn (2002), Nearshore physical processes and bio-optical properties in the New York Bight, *J. Geophys. Res.*, 107(C9), 3133, doi:10.1029/2001JC001018.
- Chant, R. J., S. Glenn, and J. Kohut (2004), Flow reversals during upwelling conditions on the New Jersey inner shelf, *J. Geophys. Res.*, 109, C12S03, doi:10.1029/2003JC001941.
- Cohn, S. E., A. da Silva, J. Guo, M. Sienkiewicz, and D. Lamich (1998), Assessing the effects of data selection with the DAO Physical-space Statistical Analysis System, *Mon. Weather Rev.*, 126, 2913–2926.
- Daley, R. (1991), *Atmospheric Data Analysis*, 457 pp., Cambridge Univ. Press, New York.
- Dinniman, M. S., J. M. Klinck, and W. O. Smith Jr. (2003), Cross shelf exchange in a model of the Ross Sea circulation and biogeochemistry, *Deep Sea Res., Part II*, 50, 3103–3120.
- Dombrowsky, E., and P. De Mey (1992), Continuous assimilation in an open domain of the northeast Atlantic: 1. Methodology and application to Athena-88, *J. Geophys. Res.*, 97, 9719–9731.
- Durski, S. M., S. M. Glenn, and D. B. Haidvogel (2004), Vertical mixing schemes in the coastal ocean: Comparison of the level 2.5 Mellor-Yamada scheme with an enhanced version of the K profile parameterization, *J. Geophys. Res.*, 109, C01015, doi:10.1029/2002JC001702.
- Fairall, C., E. Bradley, D. Rogers, J. Edson, and G. Young (1996), Bulk parameterization of air-sea fluxes for Tropical Ocean-Global Atmosphere Coupled-Ocean Atmosphere Response Experiment, *J. Geophys. Res.*, 101, 3747–3764.
- Haidvogel, D. B., H. G. Arango, K. Hedström, A. Beckmann, P. Malanotte-Rizzoli, and A. F. Shchepetkin (2000), Model evaluation experiments in the North Atlantic Basin: Simulations in nonlinear terrain-following coordinates, *Dyn. Atmos. Oceans*, 32, 239–281.
- Hodur, R. M., J. Pullen, J. Cummings, X. Hong, J. D. Doyle, P. J. Martin, and M. A. Rennick (2002), The Coupled Ocean/Atmospheric Mesoscale Prediction System (COAMPS), *Oceanography*, 15, 88–98.
- Keen, T. R., and S. M. Glenn (1995), A coupled hydrodynamic–bottom boundary layer model of storm and tidal flow in the Middle Atlantic Bight of North America, *J. Phys. Oceanogr.*, 25, 391–406.
- Kohut, J. T., S. M. Glenn, and R. J. Chant (2004), Seasonal current variability on the New Jersey inner shelf, *J. Geophys. Res.*, 109, C07S07, doi:10.1029/2003JC001963.
- Large, W. G., J. C. McWilliams, and S. C. Doney (1994), Oceanic vertical mixing: A review and a model with a nonlocal boundary layer parameterization, *Rev. Geophys.*, 32, 363–403.
- Luettich, R. A., J. J. Westerink, and N. W. Scheffner (1992), ADCIRC: An advanced three-dimensional circulation model for shelves, coasts, and estuaries, *Tech. Rep. DRP-92-6*, U.S. Army Eng. Waterw. Exper. Stat., Vicksburg, Miss.
- Lutjeharms, J. R. E., P. Penven, and C. Roy (2003), Modelling the shear edge eddies of the southern Agulhas Current, *Cont. Shelf Res.*, 23, 1099–1115.
- MacCready, P., and W. R. Geyer (2001), Estuarine salt flux through an isohaline surface, *J. Geophys. Res.*, 106, 11,629–11,637.
- Marchesiello, P., J. C. McWilliams, and A. Shchepetkin (2001), Open boundary conditions for long-term integration of regional ocean models, *Ocean Modell.*, 3, 1–20.
- Marchesiello, P., J. C. McWilliams, and A. Shchepetkin (2003), Equilibrium structure and dynamics of the California current system, *J. Phys. Oceanogr.*, 33, 753–783.
- McIntosh, P. C. (1990), Oceanographic data interpolation: Objective analysis and splines, *J. Geophys. Res.*, 95, 13,529–13,541.
- Mellor, G. L., and T. Yamada (1982), Development of a turbulence closure model for geophysical fluid problems, *Rev. Geophys.*, 20, 851–875.
- Moore, A. M., H. G. Arango, A. J. Miller, B. D. Cornuelle, E. Di Lorenzo, and D. J. Neilson (2004), A comprehensive ocean prediction and analysis system based on the tangent linear and adjoint components of a regional ocean model, *Ocean Modell.*, 7, 227–258.
- Munchow, A., and R. J. Chant (2000), Kinematics of inner shelf motion during the summer stratified season off New Jersey, *J. Phys. Oceanogr.*, 30, 247–268.
- Oke, P. R., J. S. Allen, R. N. Miller, G. D. Egbert, J. A. Austin, J. A. Barth, T. J. Boyd, P. M. Kosro, and M. D. Levine (2002a), A modeling study of the three-dimensional continental shelf circulation off Oregon. part I: Model-data comparisons, *J. Phys. Oceanogr.*, 32, 1360–1382.
- Oke, P. R., J. S. Allen, R. N. Miller, G. D. Egbert, and P. M. Kosro (2002b), Assimilation of surface velocity data into a primitive equation coastal ocean model, *J. Geophys. Res.*, 107(C9), 3122, doi:10.1029/2000JC000511.
- Paduan, J. D., and I. Shulman (2004), HF radar data assimilation in the Monterey Bay area, *J. Geophys. Res.*, 109, C07S09, doi:10.1029/2003JC001949.
- Peliz, A., J. Dubert, D. B. Haidvogel, and B. Le Cann (2003), Generation and unstable evolution of a density-driven Eastern Poleward Current: The Iberian Poleward Current, *J. Geophys. Res.*, 108(C8), 3268, doi:10.1029/2002JC001443.
- Shchepetkin, A. F., and J. C. McWilliams (1998), Quasi-monotone advection schemes based on explicit locally adaptive dissipation, *Mon. Weather Rev.*, 126, 1541–1580.
- Shchepetkin, A. F., and J. C. McWilliams (2003), A method for computing horizontal pressure-gradient force in an oceanic model with a nonaligned vertical coordinate, *J. Geophys. Res.*, 108(C3), 3090, doi:10.1029/2001JC001047.
- Shchepetkin, A. F., and J. C. McWilliams (2005), The Regional Ocean Modeling System: A split-explicit, free-surface, topography following coordinates ocean model, *Ocean Modell.*, 9, 347–404.
- Umlauf, L., and H. Burchard (2003), A generic length-scale equation for geophysical turbulence models, *J. Mar. Res.*, 61, 235–265.
- Warner, J. C., C. R. Sherwood, H. G. Arango, R. P. Signell, and B. Butman (2005), Performance of four turbulence closure methods implemented with a generic length scale method, *Ocean Modell.*, 8, 81–113.

H. G. Arango, S. M. Glenn, D. B. Haidvogel, and J. L. Wilkin, Institute of Marine and Coastal Sciences, Rutgers University, 71 Dudley Road, New Brunswick, NJ 08901-8521, USA. (arango@marine.rutgers.edu; glenn@marine.rutgers.edu; dale@marine.rutgers.edu; wilkin@marine.rutgers.edu)

K. S. Hedström, Arctic Regions Supercomputing Center, P.O. Box 756020, Fairbanks, AK 99775, USA. (kate@arsc.edu)

C. S. Lichtenwalner, College of Marine Science, University of South Florida, 140 7th Avenue South, St. Petersburg, FL 33701, USA. (clichten@seas.marine.usf.edu)